Intrinsic space charge layers and field enhancement in ferroelectric nanojunctions

Ye Cao, Anton V. Ievlev, Anna N. Morozovska, Long-Qing Chen, Sergei V. Kalinin, and Petro Maksymovych

Intrinsic space charge layers and field enhancement in ferroelectric nanojunctions

Ye Cao,[1] Anton V. Ievlev,[1] Anna N. Morozovska,[2] Long-Qing Chen,[3] Sergei V. Kalinin,[1] and Petro Maksymovych[1]

[1]*Center for Nanophase Materials Sciences, Oak Ridge National Laboratory, Oak Ridge, Tennessee 37831, USA*
[2]*Institute of Physics, National Academy of Science of Ukraine, 46, pr. Nauki, 03028 Kiev, Ukraine*
[3]*Department of Material Sciences and Engineering, The Pennsylvania State University, University Park, Pennsylvania 16802, USA*

Conducting characteristics of topological defects in ferroelectric materials, such as charged domain walls, engendered a broad interest on their scientific merit and the possibility of novel applications utilizing domain engineering. At the same time, the problem of electron transport in ferroelectrics still remains full of unanswered questions and becomes yet more relevant over the growing interest in ferroelectric semiconductors and new improper ferroelectric materials. We have employed self-consistent phase-field modeling to investigate the physical properties of a local metal-ferroelectric ($Pb(Zr_{0.2}Ti_{0.8})O_3$) junction in applied electric field. We revealed an up to 10-fold local enhancement of electric field realized by large polarization gradient and over-polarization effects due to inherent non-linear dielectric properties of $Pb(Zr_{0.2}Ti_{0.8})O_3$. The effect is independent of bias polarity and maintains its strength prior, during and after ferroelectric switching. The observed field enhancement can be considered on similar grounds as increased doping level, giving rise to reduced switching bias and threshold voltages for charge injection, electrochemical and photoelectrochemical processes. © 2015 AIP Publishing LLC. [http://dx.doi.org/10.1063/1.4926329]

Ferroelectric materials have been widely utilized in various electronic devices such as memories, piezoelectric actuators/sensors, and dielectric/ferroelectric capacitors.[1] Although generally considered insulators, many ferroelectrics are wide-band-gap semiconductors. Semiconducting properties may lead to breakdown[2] and therefore a negative impact on applications that rely on polarization switching. On the other hand, the unique properties of ferroelectric semiconductors, such as the bulk photovoltaic effect,[3–5] make them desirable for solar energy and solar fuel applications.[6–9] Moreover, ferroelectric domain walls can be conducting in ferroelectrics, most likely due to interplay between ferroelectric and semiconducting properties.[10–17]

The distinctive property of ferroelectrics is a non-linear dielectric constant due to the electric-field dependence of spontaneous polarization. In this case, an internal electric field from the space-charge layer of the Schottky contact will produce an overall non-uniform spontaneous polarization inside the film, which will in-turn influence the Schottky barrier itself. This is the basic idea behind the ferroelectric Schottky diode by Blom *et al.*[18] More recently, Xiao *et al.*[19,20] and Morozovska *et al.*[17] analyzed charge carrier accumulation at domain walls, while Zubko *et al.* revealed that increasing dopant density suppresses both coercive field and spontaneous polarization and more intriguingly produces polarization waves inside the ferroelectric.[21]

In this paper, we analyze the properties of a *local* metal-ferroelectric contact, where an inhomogeneous electric field is produced by confined electrostatic potential in plane of the surface. The latter approximates the geometry found in scanning probe microscopy (SPM), nanoscale capacitors and

may very-well correspond to the case of a macroscopic, but structurally non-uniform electrode-ferroelectric interface. The ferroelectric volume itself contains no mobile charge. By employing phase-field modeling,[22] we find that local metal-ferroelectric $Pb(Zr_{0.2}Ti_{0.8})O_3$ (PZT in short) nanojunctions produce up to 10-fold enhancement of local electric field when compared to a parallel plate capacitor. This effect may explain some of the puzzles in recent electron transport measurements on ferroelectrics and necessitates further understanding of coupled electronic-electrochemical processes in ferroelectric nanocontacts.

In the phase-field simulation, the temporal evolution of ferroelectric polarization vector is modeled by numerically solving the time-dependent Landau-Ginzburg-Devonshire (LGD) equations[23]

$$\frac{\partial P_i(\boldsymbol{x},t)}{\partial t} = -L\frac{\delta F}{\delta P_i(\boldsymbol{x},t)}, \quad i = 1, 2, 3, \quad (1)$$

in which P_i is the polarization vector, t is the time, L is the kinetic coefficient related to the domain movement, and F is the total free energy which can be expressed as

$$F = \int_V [f_{\text{lan}}(P_i) + f_{\text{grad}}(P_{i,j}) + f_{\text{elas}}(P_i, \varepsilon_{ij}) + f_{\text{elec}}(P_i, E_i)]dV, \quad (2)$$

in which $f_{\text{lan}}(P_i)$, $f_{\text{grad}}(P_{i,j})$, $f_{\text{elas}}(P_i, \varepsilon_{ij})$, and $f_{\text{elec}}(P_i, E_i)$ represent the LGD free energy density, the gradient energy density, the elastic energy density, and the electrostatic energy density, respectively. Details of each of the energy density expressions are from literature[24,25] and listed in the supplementary material.[26] Note that the surface energy is not

included in Eq. (2) as we assume natural boundary conditions (i.e., infinite extrapolation length).

To model a local contact of an SPM probe, we specify the electric potential distribution on the bottom and top interfaces of the film, respectively, as[27]

$$\phi_{\text{bottom}}(x,y) = 0,$$

$$\phi_{\text{top}}(x,y) = \phi_0 \frac{\gamma^2}{(x-x_0)^2 + (y-y_0)^2 + \gamma^2}, \quad (3)$$

in which ϕ_0 is the tip bias, (x_0, y_0) is the tip position, and γ is the half width of the tip (assumed $\gamma = 5$ nm).

We then set up periodic boundary conditions along x and y, and a general boundary condition along z directions. The simulation size is discretized into a realistic 3D mesh of $64\Delta x \times 64\Delta y \times 32\Delta z$, with $\Delta x = \Delta y = 1.0$ nm. The grid size along z direction is non-uniform. A semi-implicit spectral method[28] combined with Chebyshev collocation method[29,30] have been employed to solve the LGD equation (Eq. (1)). The simulation is conducted at room temperature $(T = 25\,^\circ\text{C})$. Detailed numerical parameters are given in the supplementary material.[26] The lattice mismatch between the film and the substrate induces an in-plane compressive strain of -0.015. The background dielectric permittivity of PZT is on the order of 5–7.[31–34] However, to compare with experimental results from real samples, we used background dielectric permittivity of 50 as suggested from the literature.[35] This is because any polarizable imperfections in real materials would be equivalent to increased dielectric permittivity. Assuming an order of magnitude smaller permittivity does not change obtained results qualitatively.

We calculated a 32 nm-thick Pb(Zr$_{0.2}$Ti$_{0.8}$)O$_3$ thin film consisting of a single tetragonal domain (along $+z$). The initial polarization is equal to $P_s = 0.7$ C/m^2. The tip bias was then increased from 0.5 to 5 V. Figs. 1(a) and 1(b) show the 2D profile (x-z plane) of polarization component (P_z) at equilibrium state under (a) 0.5 V and (b) 2 V tip bias, while Fig. 1(c) shows the state before the switched nanodomain reached the bottom surface under 5 V (c). At 0.5 V, the polarization component P_z was compressed under the tip but not switched; when the bias reached 2 V, local switching occurred in the vicinity of the tip. The switched nanodomain was in a half-prolate shape, inhibited by the large electrostatic energy penalty to propagate through the entire film. At 5 V, the nucleated nanodomain developed a cone-like morphology, reached the bottom surface, and eventually widened into a cylindrical domain. Fig. 1(e) compares the polarization induced bound charges ($-dP_z/dz$) under three biases. The local maximum of polarization charge was located at the nanodomain apex and reached as high as 10^2 C/cm^3 at 2 V and 5 V tip biases. This is due to the formation of a head-to-head tilted domain wall, where the apex region (wall tilt angle $\theta = 90^\circ$) exhibited maximum polarization charges.[17] The polarization charge at 0.5 V was an order of magnitude smaller than at 2 V and 5 V due to locally compressed but still unswitched ferroelectric polarization (Fig. 1(d)).

The 1D profiles of electric potential (ϕ) and field component along z (E_z) are compared in Figs. 1(f) and 1(g). At 0.5 V, the electric potential profile becomes non-linear, and the maximum E_z is found right under the tip. The potential profile can be well fitted by a 2nd order polynomial between the surface and $\sim$4.0 nm away from the surface. This indicates a space charge region near the tip, which screens the applied potential even in the absence of extrinsic dopants. At 2 V and 5 V, an extra "bump" near the nucleus apex is also seen in the potential profile (red and green lines in Fig. 1(f)), resulting in an extra local field maximum at the apex (Fig. 1(g)). The
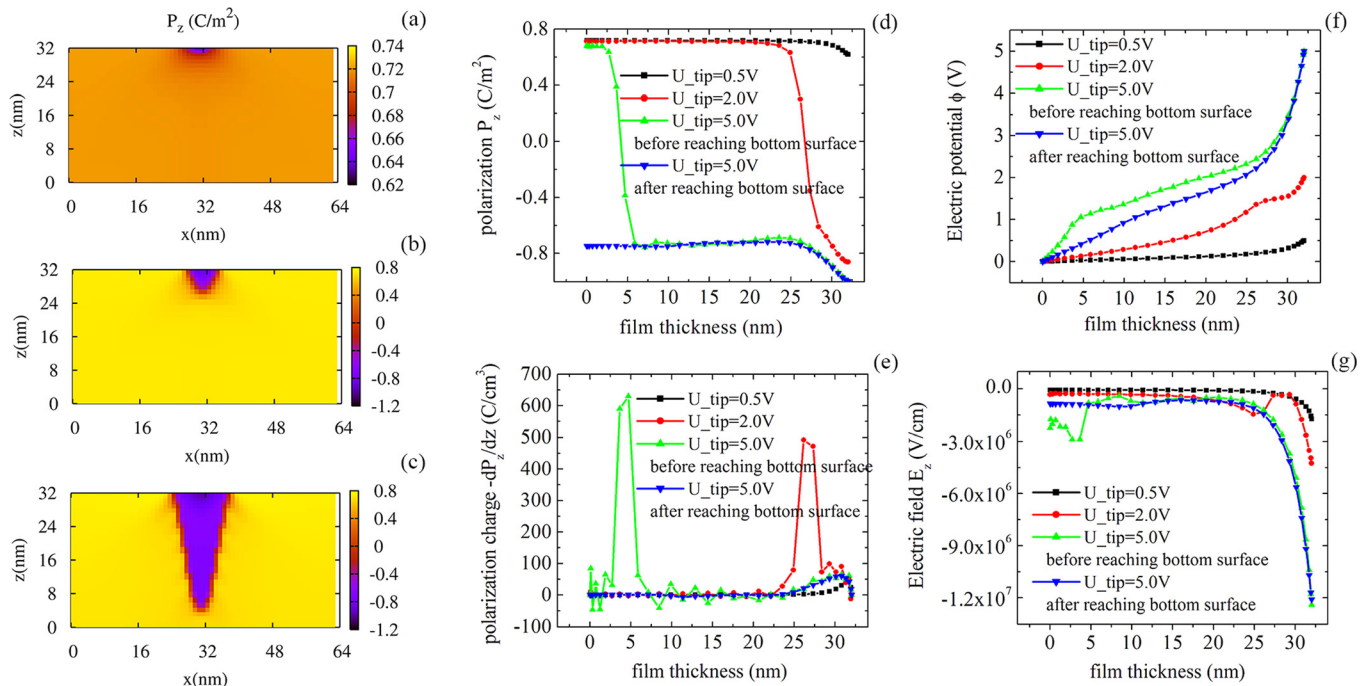
FIG. 1. 2D plot of the steady state distribution of ferroelectric polarization component P_z in the x-z plane under tip bias of 0.5 V (a) and 2 V (b), and of a state before the nucleated nanodomain propagates into a cylindrical domain configuration under tip bias of 5 V (c). 1D z-profiles of spontaneous polarization (P_z) (d), polarization induced bound charge (e), electric potential (f), and electric field component (E_z) at tip biases of 0.5, 2, and 5 V. Z-profiles are taken at the center of the film in the x-y plane.
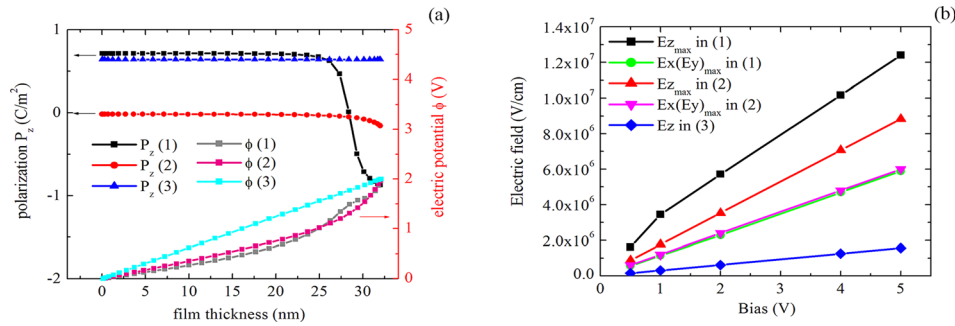
FIG. 2. (a) Comparison of polarization profile (P_z) and electric potential distribution (ϕ) in three scenarios: (1) ferroelectric single domain (P_z +) PZT under a tip bias; (2) linear dielectrics under exactly same tip geometry as (1); and (3) ferroelectric single domain (P_z +) PZT under a uniform plate electrode. (b) Comparison of local maximum electric field in the vicinity of the surface (both in-plane (E_x, E_y) and out-of-plane (E_z)) for scenarios (1) and (2), and the calculated average field (E_z only) in scenario (3) at different biases from 0.5 V to 5 V.

potential "bump" and the local field maximum near apex promoted the nanodomain growth and eventually disappeared at 5 V when they reached the bottom electrode.

To further understand the effect of local electric field on nanojunction switching, we considered three scenarios: (1) ferroelectric single domain (P_z +) PZT under a tip bias; (2) linear dielectrics under the same tip as (1); and (3) ferroelectric single domain (P_z +) PZT under a uniform plate electrode. In a linear dielectric, the polarization is related to the electric field as

$$P_i = \varepsilon_0 \chi_{ij} E_j = \varepsilon_0 (\kappa_{ij} - 1) E_j, \tag{4}$$

in which χ_{ij} is the susceptibility tensor, and the polarization and electric potential were obtained by solving the coupled equations (5), (S-9), and (S-12).[26] For comparison between scenarios (1) and (2), we assumed $\kappa_{ij} = 50 \cdot \delta_{ij}$ (δ_{ij} is the Delta-Kroneker symbol) in linear dielectrics. Fig. 2(a) illustrates the 1D profiles of the polarization component P_z and electric potential of (1)–(3) at 2 V. Compared to ferroelectric PZT under tip (1), P_z in linear dielectrics (2) was locally compressed under the tip and remained constant away from the tip, resulting in a much smaller polarization gradient and thus smaller polarization charges under the tip. The electric potential in (2) showed no "bump" and had smaller gradient under the tip than in (1). In scenario (3), P_z remained constant throughout the film and reduced from its equilibrium value (~0.7 C/m^2 under -1.5% substrate strains without applied bias) by ~0.06 C/m^2. No local switching occurred and the electric potential linearly dropped from top to bottom surfaces. Fig. 2(b) compares the local maximum field at different biases from 0.5 to 5 V for both in-plane (E_x, E_y) and out-of-plane (E_z) field components in scenarios (1) and (2), and an out-of-plane field component (E_z) for scenario (3). While E_x (E_y) are almost identical in (1) and (2), E_z in (2) is much smaller than in (1) at each bias. This is consistent with Fig. 2(a). It is also found out that E_z under the tip reached 1 V/nm at 5 V bias, almost ten times larger than the average field under the uniform electrode (3). This field enhancement indicates that the switching bias could be significantly reduced under a tip-geometry bias.

The large enhancement of local electric field due to lattice polarization effect will naturally translate into a very large enhancement of efficiency of charge injection. Here, we estimated the transmission coefficient (T_{WKB}) of the Fowler-Nordheim tunneling model based on the simulated

electric potential profiles shown in a simplified tip-surface junction (Fig. 3(a)). We calculated the WKB approximated transmission coefficient (T_{WKB}) along z direction for barrier widths defined by the potential profiles in scenarios (1)–(3) based on the following equation assuming barrier height $q_0\phi(z)|_{z\,\text{at the interface}} - E = 0.5\,\text{eV}$:

$$T_{WKB} = \exp\left[-\frac{2\sqrt{2m}}{\hbar \int_{\phi(z)>E} dx \sqrt{q_0\phi(z) - E}}\right], \tag{5}$$

in which m is the electron mass, $\hbar$ is the reduced Planck constant, q_0 is the unit charge, $\phi(z)$ is the electric potential along z, and E is the work function of the electrode. From Fig. 3(c), it is seen that T_{WKB} in PZT under uniform plate electrode are several orders of magnitude smaller than those in PZT and linear dielectrics under tip biases.

Our computational findings may therefore be relevant to a well-known problem with the description of Schottky barriers in ferroelectric oxides. It has been known for some time that the leakage current observed in macroscopic capacitors typically requires about 10-fold larger electric fields than what would be expected based on intentional or unintentional doping levels.[36] Likewise, in more than a few works utilizing SPM methods, the results could only be explained by comparatively high electric fields in the range of 0.1–1 V/nm. These include the observation of intrinsic ferroelectric switching in BiFeO$_3$[37] and polarization-controlled Schottky barriers in PZT.[38]

There are several ways by which the required large electric field can arise, particularly in SPM geometry. The simplest assumption is that of a small size of the contact area that leads to large geometric enhancing of the electric field. As some of us have shown earlier,[38] the I-V curves can be reasonably well-fit with the Fowler-Nordheim tunneling equation and SPM tips with a radius of 2–5 nm, which may correspond, for example, to a sharp asperity at the tip apex. Another way to introduce high electric field is to consider doping levels in excess of $1 \times 10^{19}\,\text{cm}^{-3}$. In Fig. 3(d), we show fitting of the representative I-V curves from a 30 nm film of PZT[14] using 1D Fowler-Nordheim tunneling model and the Schottky contact with the maximum electric field determined by[39,40]

$$E_m = \sqrt{\frac{2e_0 N_D (V + V_{bi})}{\varepsilon_0 \kappa}}, \tag{6}$$
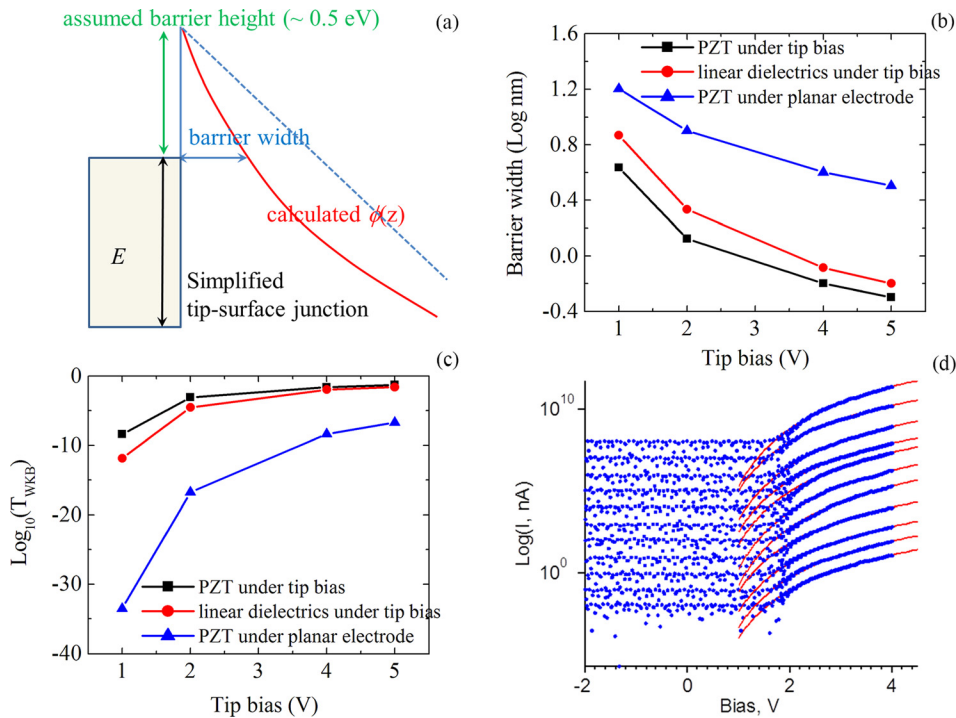
FIG. 3. (a) Schematic illustration of the tunneling barrier assumed in the calculation of the transmission coefficient (T_{WKB}). Barrier width (b) and transmission coefficient (T_{WKB}) (c) as a function of bias in the dielectric nanojunctions with ferroelectric PZT, linear dielectrics under exactly same tip and ferroelectric PZT under uniform planar electrode; (d) Fitting of representative I-V curves measured on the surface of the upward-polarized 30 nm Pb(Zr$_{0.2}$Ti$_{0.8}$)O$_3$ film[14] at 300 K in ultra-high vacuum. I-V curves (blue) offset for clarity. Each fit (red line) corresponds to 1D Fowler-Nordheim tunneling model with the electric field obtained with Eq. (6).

where e_0 is the unite charge, N_D is the doping level, V and V_{bi} are the applied bias and built-in potential, respectively, and ε_0 and κ are vacuum and dielectric permittivity, respectively. Here, we assume that the tunneling barrier is resistance limiting, which is valid in the regime of low tunneling current. The fits are generally satisfactory, although there is significant uncertainty in the tip radius. Nevertheless, in most cases that radius exceeds 10 nm, which is much more reasonable for a local junction. However, this also necessitates the doping levels of $\sim 4 \times 10^{19}$ cm^{-3} for a barrier height of ~ 0.8 eV. Reasonably good fits can be obtained for even larger barrier height, but still larger doping levels are required to achieve the field of 0.2–0.5 V/nm. Although these doping levels may not be unrealistic, one needs to consider whether at some point there will be a transition to metallic conductivity given that the Mott criterion for BaTiO$_3$ is satisfied at $\sim 5 \times 10^{18}$ cm^{-3}.[41]

The mechanism presented in this paper can relieve some of the above constraints by providing electric field enhancement through over-polarization effects. In fact, it is clear from Fig. 3(d) that the "missing" 10-fold enhancement is readily produced by dielectric junctions. It will be interesting in the future to model ferroelectric semiconductors in a similar fashion to observe the interplay between external bias-induced and internal space-charge induced over-polarization effects, which may be relevant for piezoelectric applications and other reasonably low-field operation regimes where the film is far from full depletion.

In summary, we implemented a phase-field method to study the ferroelectric switching dynamics in the local electric field applied to strained PZT thin film. It was revealed that ferroelectric polarization responded to applied field by over-polarization and therefore occurrence of space-charge layer solely due to polarization gradient. This effect enhances local electric fields by as much as a factor of 10 relative to parallel plate capacitor and is largely insensitive to the exact polarization structure in the ferroelectric volume. The field enhancement dramatically lowers the voltage threshold for both charge injection as well as ferroelectric switching, which may be beneficial for certain cases but also detrimental if charge-injection precedes material breakdown.

[1] O. Auciello, J. F. Scott, and R. Ramesh, Phys. Today **51**(7), 22 (1998).
[2] V. M. Fridkin, *Ferroelectric Semiconductors* (Consultants Bureau, New York, London, 1980).

[3]T. Choi, S. Lee, Y. J. Choi, V. Kiryukhin, and S. W. Cheong, Science **324**, 63 (2009).

[4]I. Grinberg, D. V. West, M. Torres, G. Y. Gou, D. M. Stein, L. Y. Wu, G. N. Chen, E. M. Gallo, A. R. Akbashev, P. K. Davies, J. E. Spanier, and A. M. Rappe, Nature **503**, 509 (2013).

[5]S. Y. Yang, J. Seidel, S. J. Byrnes, P. Shafer, C. H. Yang, M. D. Rossell, P. Yu, Y. H. Chu, J. F. Scott, J. W. Ager, L. W. Martin, and R. Ramesh, Nat. Nanotechnol. **5**, 143 (2010).

[6]S. Y. Yang, L. W. Martin, S. J. Byrnes, T. E. Conry, S. R. Basu, D. Paran, L. Reichertz, J. Ihlefeld, C. Adamo, A. Melville, Y. H. Chu, C. H. Yang, J. L. Musfeldt, D. G. Schlom, J. W. Ager, and R. Ramesh, Appl. Phys. Lett. **95**, 062909 (2009).

[7]S. M. Young and A. M. Rappe, Phys. Rev. Lett. **109**, 116601 (2012).

[8]L. Jiang, I. Grinberg, F. G. Wang, S. M. Young, P. K. Davies, and A. M. Rappe, Phys. Rev. B **90**, 075153 (2014).

[9]F. G. Wang and A. M. Rappe, Phys. Rev. B **91**, 165124 (2015).

[10]B. M. Vul, G. M. Guro, and I. I. Ivanchik, Ferroelectrics **6**, 29 (1973).

[11]J. Seidel, L. W. Martin, Q. He, Q. Zhan, Y. H. Chu, A. Rother, M. E. Hawkridge, P. Maksymovych, P. Yu, M. Gajek, N. Balke, S. V. Kalinin, S. Gemming, F. Wang, G. Catalan, J. F. Scott, N. A. Spaldin, J. Orenstein, and R. Ramesh, Nat. Mater. **8**, 229 (2009).

[12]N. Balke, B. Winchester, W. Ren, Y. H. Chu, A. N. Morozovska, E. A. Eliseev, M. Huijben, R. K. Vasudevan, P. Maksymovych, J. Britson, S. Jesse, I. Kornev, R. Ramesh, L. Bellaiche, L. Q. Chen, and S. V. Kalinin, Nat. Phys. **8**, 81 (2012).

[13]P. Maksymovych, J. Seidel, Y. H. Chu, P. P. Wu, A. P. Baddorf, L. Q. Chen, S. V. Kalinin, and R. Ramesh, Nano Lett. **11**, 1906 (2011).

[14]P. Maksymovych, A. N. Morozovska, P. Yu, E. A. Eliseev, Y. H. Chu, R. Ramesh, A. P. Baddorf, and S. V. Kalinin, Nano Lett. **12**, 209 (2012).

[15]J. K. Lee, G. Y. Shin, K. Song, W. S. Choi, Y. A. Shin, S. Y. Park, J. Britson, Y. Cao, L. Q. Chen, H. N. Lee, and S. H. Oh, Acta Mater. **61**, 6765 (2013).

[16]M. Y. Gureev, A. K. Tagantsev, and N. Setter, Phys. Rev. B **83**, 184104 (2011).

[17]E. A. Eliseev, A. N. Morozovska, G. S. Svechnikov, V. Gopalan, and V. Y. Shur, Phys. Rev. B **83**, 235313 (2011).

[18]P. W. M. Blom, R. M. Wolf, J. F. M. Cillessen, and M. P. C. M. Krijn, Phys. Rev. Lett. **73**, 2107 (1994).

[19]Y. Xiao, V. B. Shenoy, and K. Bhattacharya, Phys. Rev. Lett. **95**, 247603 (2005).

[20]V. B. Shenoy, Y. Xiao, and K. Bhattacharya, J. Appl. Phys. **111**, 084105 (2012).

[21]P. Zubko, D. J. Jung, and J. F. Scott, J. Appl. Phys. **100**, 114112 (2006).

[22]H. L. Hu and L. Q. Chen, Mater. Sci. Eng., A **238**, 182 (1997).

[23]L. Q. Chen, J. Am. Ceram. Soc. **91**, 1835 (2008).

[24]Y. L. Li, S. Y. Hu, Z. K. Liu, and L. Q. Chen, Appl. Phys. Lett. **78**, 3878 (2001).

[25]Y. L. Li, S. Y. Hu, Z. K. Liu, and L. Q. Chen, Acta Mater. **50**, 395 (2002).

[26]See supplementary material at http://dx.doi.org/10.1063/1.4926329 for detailed formulation and parameters used in the phase-field simulation.

[27]S. Choudhury, J. X. Zhang, Y. L. Li, L. Q. Chen, Q. X. Jia, and S. V. Kalinin, Appl. Phys. Lett. **93**, 162901 (2008).

[28]L. Q. Chen and J. Shen, Comput. Phys. Commun. **108**, 147 (1998).

[29]Y. Cao, S. Bhattacharya, J. Shen, C. A. Randall, and L. Q. Chen, J. Appl. Phys. **114**, 224102 (2013).

[30]Y. Cao, J. Shen, C. Randall, and L. Q. Chen, J. Am. Ceram. Soc. **97**, 3568 (2014).

[31]A. K. Tagantsev and G. Gerra, J. Appl. Phys. **100**, 051607 (2006).

[32]A. K. Tagantsev, Ferroelectrics **375**, 19 (2008).

[33]A. K. Tagantsev, G. Gerra, and N. Setter, Phys. Rev. B **77**, 174111 (2008).

[34]A. N. Morozovska, E. A. Eliseev, S. V. Svechnikov, A. D. Krutov, V. Y. Shur, A. Y. Borisevich, P. Maksymovych, and S. V. Kalinin, Phys. Rev. B **81**, 205308 (2010).

[35]G. Rupprecht and R. O. Bell, Phys. Rev. **135**, A748 (1964).

[36]M. Dawber and J. F. Scott, Appl. Phys. Lett. **76**, 1060 (2000).

[37]P. Maksymovych, S. Jesse, M. Huijben, R. Ramesh, A. Morozovska, S. Choudhury, L. Q. Chen, A. P. Baddorf, and S. V. Kalinin, Phys. Rev. Lett. **102**, 017601 (2009).

[38]P. Maksymovych, S. Jesse, P. Yu, R. Ramesh, A. P. Baddorf, and S. V. Kalinin, Science **324**, 1421 (2009).

[39]L. Pintilie and M. Alexe, J. Appl. Phys. **98**, 124103 (2005).

[40]L. Pintilie, I. Boerasu, M. J. M. Gomes, T. Zhao, R. Ramesh, and M. Alexe, J. Appl. Phys. **98**, 124104 (2005).

[41]S. Lee, J. A. Bock, S. Trolier-McKinstry, and C. A. Randall, J. Eur. Ceram. Soc. **32**, 3971 (2012).